EDGE ARTICLE

Check for updates

All publication charges for this article have been paid for by the Royal Society of Chemistry

Mixed lead–tin perovskite films with >7 μs charge carrier lifetimes realized by maltol post-treatment†

Shuaifeng Hu, [ID] [a] Minh Anh Truong, [ID] [a] Kento Otsuka, [ID] [a] Taketo Handa, [ID] [a] Takumi Yamada, [ID] [a] Ryosuke Nishikubo, [ID] [b] Yasuko Iwasaki, [ID] [a] Akinori Saeki, [ID] [b] Richard Murdey, [ID] [a] Yoshihiko Kanemitsu [ID] [a] and Atsushi Wakamiya [ID] *[a]

Mixed lead–tin (Pb–Sn) halide perovskites with optimum band gaps near 1.3 eV are promising candidates for next-generation solar cells. However, the performance of solar cells fabricated with Pb–Sn perovskites is restricted by the facile oxidation of Sn(II) to Sn(IV), which induces self-doping. Maltol, a naturally occurring flavor enhancer and strong metal binding agent, was found to effectively suppress Sn(IV) formation and passivate defects in mixed Pb–Sn perovskite films. When used in combination with Sn(IV) scavenging, the maltol surface treatment led to high-quality perovskite films which showed enhanced photoluminescence intensities and charge carrier lifetimes in excess of 7 μs. The scavenging and surface treatments resulted in highly reproducible solar cell devices, with photoconversion efficiencies of up to 21.4% under AM1.5G illumination.

1. Introduction

Lead (Pb)-based perovskite solar cells (PSCs) have reached a power conversion efficiency (PCE) of 25.6%.[1,2] While such devices are highly optimized, the band gap of Pb-based perovskite materials (E_g > 1.45 eV)[3] actually lies slightly outside the range of maximum performance for single-junction solar cells, 1.1–1.4 eV, as determined by Shockley and Queisser.[4] The band gaps of mixed lead–tin (Pb–Sn) perovskite absorbers, meanwhile, fall within the optimal range, being typically 1.2–1.4 eV.[5,6] In the last few years, there has been remarkable progress in the development of Pb–Sn PSCs,[7–11] with cell efficiencies now reaching 21.7%.[12,13] Despite the optimal band gap, however, the reported device efficiencies[5,7,12–21] remain lower than those of their Pb-based counterparts.[1,2,22–24] One of the main impediments for any tin-containing perovskite is the facile oxidation of Sn(II) to Sn(IV). Saidaminov *et al.*[25] and Pascual *et al.*[26] found that the starting material, SnI₂, can be easily oxidized, even by the solvent used for the film fabrication (dimethyl sulfoxide, DMSO). Oxygen levels as low as a few ppm can cause Sn(II) in the perovskite films to oxidize, creating Sn(II) vacancies which lead to an increase in hole density.[27–30] This p-doping effect has a very strong negative impact on device performance.[31]

Various strategies for mitigating this issue have been proposed.[32] One effective way to reduce the Sn(IV) content in the perovskite films is to remove it from the precursor solution, by modifying the perovskite precursor solution *via* various methods. It was reported that the addition of Sn(0) powder into the Sn-containing precursor solution not only improved the purity of the precursor solution but also reduced Sn(II) vacancies in the resulting perovskite films due to extra Sn(II) generated by the reaction of Sn(IV) with metallic Sn(0).[8,9,33] Antioxidants or reducing reagents, like formamidinesulfinic acid,[12] pyrazine,[34] hydroquinone sulfonic acid,[35] and 8-hydroxyquinoline,[36] have also been found to reduce the Sn(IV) content in perovskite precursor solution.

It is also important to reduce the Sn(IV) in the starting materials used to prepare the precursor solution. To this end, we have previously developed highly purified starting materials for the fabrication of Sn-based PSCs.[37–39] We have also recently reported a Sn(IV) scavenging method based on the high chemical selectivity of an 8π electron system 1,4-bis(trimethylsilyl)-2,3,5,6-tetramethyl-1,4-dihydropyrazine (TM-DHP) for SnF₂ over SnI₂.[40] We found that when TM-DHP is added into a FA₀.₇₅MA₀.₂₅SnI₃ precursor solution in the presence of SnF₂, the Sn(II) from SnF₂ is reduced to generate Sn(0) nanoparticles. These Sn(0) nanoparticles effectively scavenge Sn(IV) impurities at the precursor preparation stage, giving Sn(IV)-free perovskites in the bulk of the obtained films.

Despite these notable improvements to the quality of the as-fabricated materials, the perovskite films remain vulnerable to oxidation after fabrication, especially at the exposed surfaces.[41] To address this, post-treatments for the perovskite films have been developed to protect and passivate the perovskite

[a]Institute for Chemical Research, Kyoto University, Gokasho, Uji, Kyoto 611-0011, Japan. E-mail: wakamiya@scl.kyoto-u.ac.jp

[b]Department of Applied Chemistry, Graduate School of Engineering, Osaka University, 2-1 Yamadaoka, Suita, Osaka 565-0871, Japan

surfaces.[42] From a chemical point of view, a strong chelating agent would be a good choice to stabilize the Sn(II) species. Kamarudin *et al.* reported that amine groups in ethylenediamine bind to the undercoordinated Sn(II) species on the Sn perovskite surface, resulting in improved stability towards oxidation.[43] Unfortunately, however, the high basicity of the ethylenediamine resulted in damage to the Sn perovskite films.[44,45] Milder, but effective reagents are therefore desirable for the post-treatment of the Sn-containing perovskite films. Among the candidates, the environmental-friendly molecule; 3-hydroxy-2-methyl-4-pyrone (maltol), known as a 'flavor enhancer', is a promising candidate due to its noteworthy metal chelating ability.[46]

In this work, we extend the use of the Sn(IV) scavenging method to mixed Pb–Sn perovskite system, and introduce an additional post-treatment of the perovskite surface with maltol. The maltol treatment was found to suppress Sn(II) oxidation and reduce the density of defects at the perovskite film surface. The photoluminescence (PL) lifetime increasing from 1.3 to 7.4 μs accompanied with a fivefold increase in PL intensity. The PCE of the champion device fabricated with the combination of Sn(IV) scavenging and maltol post-treatment was 21.4%.

2. Results and discussion

Maltol, $C_6H_6O_3$, is a small α-hydroxy ketone known for having an intense chemical activity towards hard metal ions. We found that the electron-rich oxygen atoms in the carbonyl and the hydroxyl groups of maltol simultaneously coordinate to the Sn(II) in SnI_2 to form SnI(maltol) complex (Fig. 1a and b). Similar complexes were observed to form with SnF_2 and $SnBr_2$ (Scheme S1 and Fig. S1–S7†). We therefore surmise that if maltol binds to the undercoordinated Sn(II) sites (Fig. 1c) at the surface of Pb–Sn perovskite films, it should effectively suppress the formation of the defects, like Sn(II) vacancies, at the perovskite film surface.

To verify this hypothesis, three kinds of perovskite samples were prepared; control films without scavenging or maltol post treatment, films prepared with TM-DHP reductant only, and films prepared with both TM-DHP reductant and maltol post-

treatment. The perovskite composition used was $Cs_{0.1}FA_{0.6}MA_{0.3}Sn_{0.5}Pb_{0.5}I_3$ (FA = formamidinium, MA = methylammonium). This composition was selected by evaluating the PL properties and valence band energy levels of a series of 25 candidate materials (Fig. S8 and S9, Table S1†). The perovskite layers were prepared by the one step method with chlorobenzene antisolvent. SnF_2 (10 mol% with respect to SnI_2) and $Pb(SCN)_2$ (2 mol% with respect to PbI_2) were added to the perovskite precursor solution. SnF_2 additive is known to suppress the oxidation of Sn(II) at the precursor preparation stage,[5] while $Pb(SCN)_2$ is commonly added to mediate the perovskite crystal growth.[18] The precursor concentration is 1.8 M, chosen based on previous reports on efficient mixed Pb–Sn PSCs.[9,18] For the samples with Sn(IV) scavenging, 1 mol% TM-DHP was added to the precursor solution as described previously.[40] For the samples with maltol post treatment, 1 mg mL^{-1} maltol dissolved in toluene was applied to the surface of the films by spin-coating, followed by annealing at 65 °C. Accordingly, the control, TM-DHP-treated, and both TM-DHP and maltol treated perovskite films were respectively prepared.

The oxidation state of Sn at the perovskite film surface was examined using X-ray photoelectron spectroscopy (XPS). Fig. 2a–c show the Sn 3d signal for the three perovskite films, which can be deconvoluted into two components; a large main peak, and a single shoulder on the high binding energy side. After peak fitting, the main peaks, centered at about 494.8 and 486.3 eV, are assigned to Sn(II), while the secondary features, at about 496.3 and 487.6 eV, are attributed to Sn(IV). The amount of Sn(IV) content at the surface of the perovskite films was 9% for the control, 6% for TM-DHP-treated films, as estimated from the ratio of the Sn(IV) peak to the total signal area. TM-DHP effectively scavenges Sn(IV) from the precursor materials, resulting in less Sn(IV) in the perovskite films. The Sn(IV) content is reduced further, to 3%, for the TM-DHP and maltol treated films. The maltol helps to decrease the Sn(IV) content by protecting and passivating the surface of the perovskite films, making it more resistant to oxidation by the environment.

The effect of the treatments on the film morphology and crystallinity were examined by the scanning electron microscopy (SEM) and X-ray diffraction (XRD), respectively. No obvious
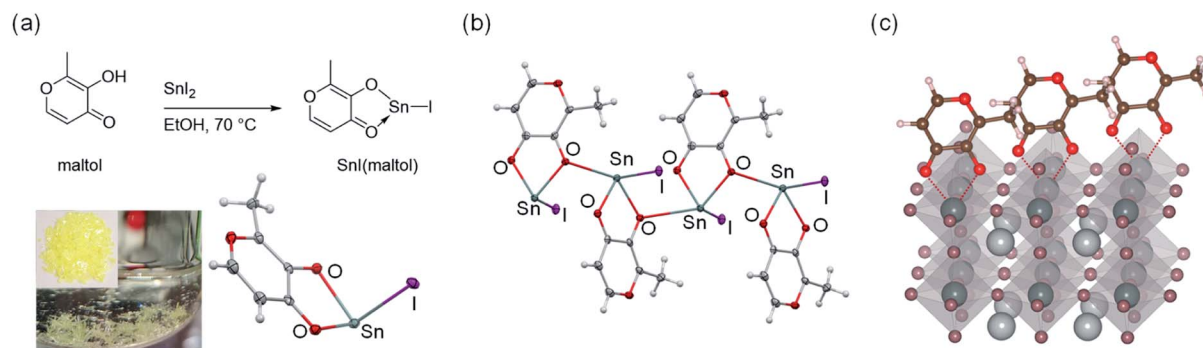

Fig. 1 (a) Synthetic route, picture of single crystals, and ORTEP drawing of SnI(maltol) crystal structure with 50% thermal ellipsoids. (b) The crystal packing structure of SnI(maltol). (c) Schematic illustration of the chelation between maltol molecules and undercoordinated Sn(II) species on the perovskite film surface.
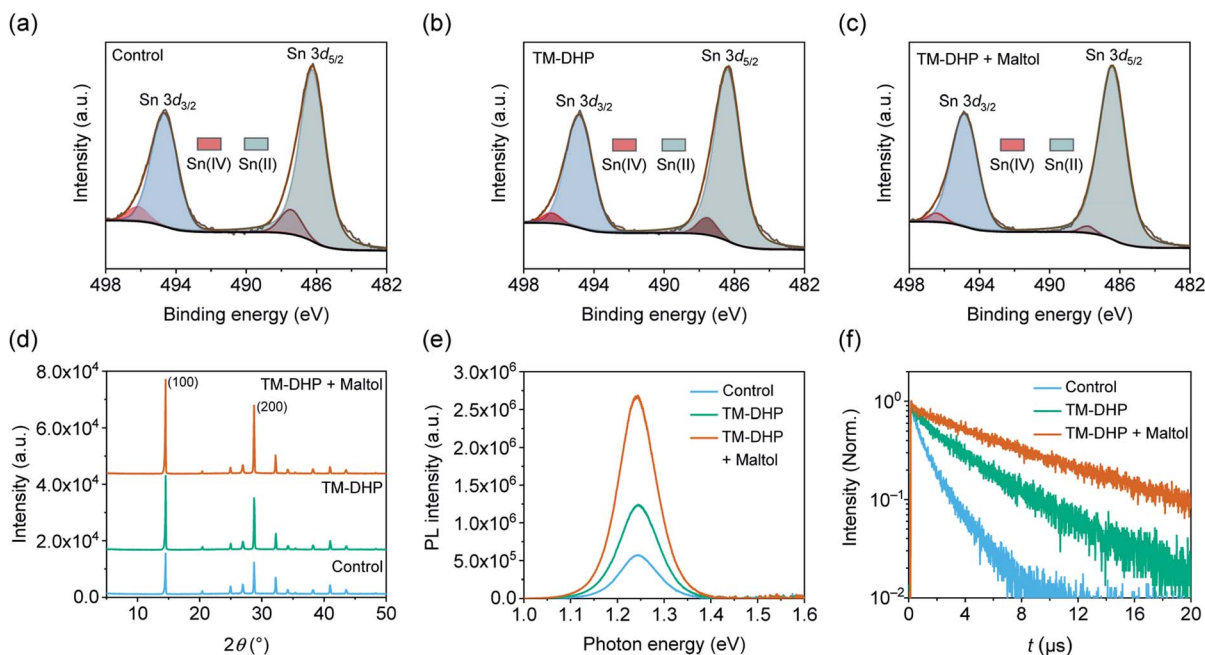
Fig. 2 XPS spectra of Sn $3d_{3/2}$ and $3d_{5/2}$ core levels for the (a) control, (b) TM-DHP-treated, and (c) TM-DHP combined with maltol treated perovskite films. The amount of Sn(IV) content on the surface of the control, TM-DHP, and both TM-DHP and maltol treated perovskite films is 9, 6, and 3%, respectively. (d) XRD patterns of perovskite films fabricated on PEDOT:PSS-coated FTO substrates. (e) Steady-state photoluminescence (PL) spectra, and (f) time-resolved photoluminescence (TRPL) decay curves of the perovskite films fabricated on quartz substrates. The carrier lifetime of the control, TM-DHP, and both TM-DHP and maltol treated perovskite films is 1.3, 3.7, and 7.4 µs, respectively.

differences in grain size or roughness can be discerned from the SEM images (Fig. S10†), and the full-width at half-maximum (FWHM) of the XRD characteristic peaks are largely unaffected by the treatments (Fig. S11†). The films treated with TM-DHP, have improved crystallinity, as indicated by the stronger intensities of the peaks at 14.5° and 28.8°, indexed to (100) and (200) planes of the perovskite, respectively (Fig. 2d). This may be the result of the mediating influence of TMP (tetramethylpyrazine), formed by the reaction of TM-DHP and SnF_2,[40] on the perovskite crystallization process.[34] The intensity of the (100) and (200) peaks increased even more after the maltol treatment, suggesting some additional improvement in film crystallinity. As the surface treatment involves washing the perovskite film with a solution of maltol dissolved in toluene, followed by a second annealing step, we speculate that the improvement in crystallinity in the treated films could be caused by structural reorganization during the annealing process.[47–49]

The treatments were found to have a considerable impact on the charge carrier recombination dynamics, which are critical for achieving efficient conversion of photons to electrical charge. As shown in Fig. 2e, the PL intensity of the perovskite film prepared with TM-DHP is 2.2 times larger than that of control film. After maltol post-treatment, the PL intensity increases to become 4.7 times stronger than the control. The increase in PL intensity indicates that non-radiative recombination is supressed, and, therefore, the trap states in the perovskite films have been reduced by both the TM-DHP treatment and the maltol post-treatment.

The reduction in charge carrier recombination is confirmed by the charge carrier lifetimes, which are estimated from the time resolved photoluminescence (TRPL) decay curves shown in Fig. 2f. These measurements were made under a photon flux of 3.5×10^{11} photons per cm^2, comparable to the incident flux under AM1.5G. The lifetimes were found to depend on the incident light intensity,[50] as shown in ESI Fig. S12 and S13.† With Sn(IV) scavenging, the lifetime increased from 1.3 to 3.7 µs. After maltol post-treatment, the lifetime reached a maximum of 7.4 µs. This is over six times longer than the value of 1.1 µs previously reported for mixed Pb–Sn perovskite films.[7] This value, obtained for thin polycrystalline Pb–Sn perovskite layers, is even comparable to those reported for state-of-the-art perovskite single crystals.[51]

Diffusion lengths could not be readily determined as we were unable to estimate the charge carrier mobility from the space-charge-limited current data.[52] Instead, an approximate evaluation of the diffusion length was realized using reported values for the diffusion coefficients (D) of Pb–Sn perovskite.[7] Using the PL lifetime, $t = 7.4$ µs, determined for our film, and their reported values of 0.02–0.05 $cm^2 \ s^{-1}$ for the diffusion coefficients, the carrier diffusion length calculated from $\sqrt{Dt}$, is estimated to fall in the range of 3.8–6.1 µm. The local mobility of the holes and electrons within individual perovskite grains can be estimated using flash-photolysis time-resolved microwave conductivity (TRMC) (Fig. S14 and S15†).[53,54] The values are estimated to be 70 $cm^2 \ V^{-1} \ s^{-1}$ and 110 $cm^2 \ V^{-1} \ s^{-1}$, respectively. These high values point to the overall high quality of the perovskite

materials, which is also supported by the XRD and PL experiments.

To confirm the impact of the improved charge carrier recombination dynamics on the device performance, the corresponding PSCs were fabricated. The solar cells had an positive–intrinsic–negative structure: fluorine-doped tin oxide (FTO)/poly(3,4-ethylenedioxythiophene):poly(styrene sulfonate) (PEDOT:PSS)/perovskite/fullerene (C_{60})/bathocuproine (BCP)/ silver (Ag) (Fig. 3a). The perovskite film thickness was 800–1000 nm. The current density–voltage (J–V) curves of the best devices are shown in Fig. 3b, and the corresponding photovoltaic parameters are listed in Table 1. Measurements were made in inert atmosphere, under AM1.5G simulated solar radiation.

For control devices prepared without the TM-DHP or maltol treatment, the highest PCE was 18.2% (forward scan, J_{SC} = 31.1 mA cm^{-2}, V_{OC} = 0.78 V, and FF = 0.75). With the TM-DHP but without maltol treatment, the forward scan J_{SC}, V_{OC}, and FF was slightly increased to 31.6 mA cm^{-2}, 0.79 V, and 0.76, respectively, and the PCE reached 19.0%. Significantly improved performance was achieved when, in addition to TM-DHP treatment, the perovskite layers were post-treated with maltol. The champion PCE was 21.4% (reverse scan, J_{SC} = 33.1 mA cm^{-2}, V_{OC} = 0.82 V, and FF = 0.79) and devices had considerably improved reproducibility (Fig. S16†). This PCE is very close to the reported best performance for mixed Pb–Sn PSCs, 21.7%.[12,13] In Fig. 3c, we can observe that the PSCs reached the

Table 1 Photovoltaic parameters of the perovskite solar cells

Device	Scan[a]	J_{SC} (mA cm^{-2})	V_{OC} (V)	FF	PCE (%)
Control	Forward	31.1	0.78	0.75	18.2
	Reverse	30.9	0.78	0.74	18.1
TM-DHP	Forward	31.6	0.79	0.76	19.0
	Reverse	31.3	0.80	0.75	18.7
TM-DHP + maltol	Forward	33.2	0.82	0.77	21.0
	Reverse	33.1	0.82	0.79	21.4

[a] Scan direction: forward and reverse denotes the scan direction from J_{SC} to V_{OC} and from V_{OC} to J_{SC}, respectively.

highest external quantum efficiency (EQE) of 91.2% at 680 nm, and the corresponding internal quantum efficiency (IQE) was 98.8%. The integrated J_{SC} was 32.3 mA cm^{-2}, somewhat lower than the maximum value (33.2 mA cm^{-2}) obtained from the J–V curves. The difference is attributed to the spectral mismatch of the solar simulator especially in near-infrared region. Considering the mismatch factor, which was calculated to be 1.027 (Fig. S17†), the J_{SC} values from the J–V curves correspond closely with the integrated value.

To investigate the improved device performance in the view of its electronic properties, additional characterizations of the devices were performed. Impedance scans (Fig. 3d and S18†) reveal a single semicircle for each device, the diameter of which
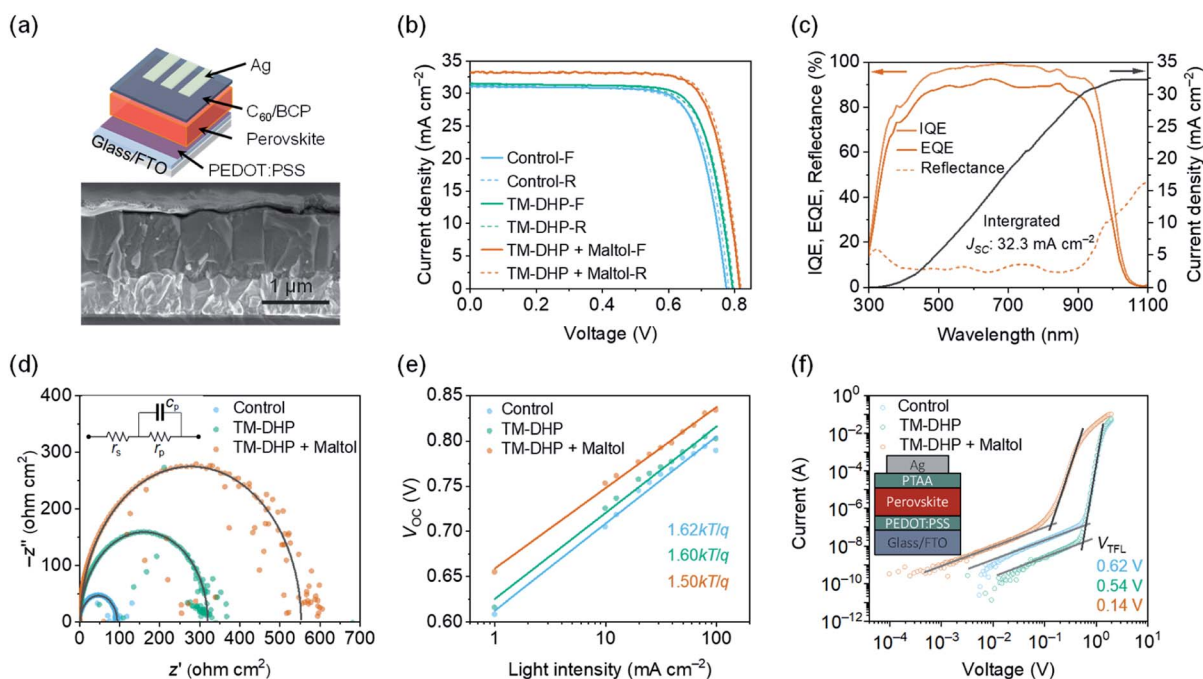

Fig. 3 (a) Schematic illustration and cross-sectional SEM image of a completed device with the architecture of FTO/PEDOT:PSS/perovskite/C_{60}/ BCP/Ag. (b) J–V curves of the PSCs. (c) IQE, EQE, reflectance spectra and integrated J_{SC} of the encapsulated champion device under AM1.5G illumination in ambient air, no antireflection technique was applied for the device fabrication. (d) Complex impedance plots of PSCs measured in inert atmosphere under AM1.5G illumination. The shunt resistance across the perovskite layer was estimated at 93, 318, and 550 Ω cm^2 for the control, TM-DHP, and both TM-DHP and maltol treated PSCs, respectively. Insert shows the equivalent circuit model for fitting the electrochemical impedance spectroscopy data. (e) The open-circuit voltage V_{OC} as a function of illumination intensity with an ideality factor of 1.62, 1.60, and 1.50 for the control, TM-DHP, and both TM-DHP and maltol treated PSCs, respectively. (f) Dark current–voltage curves of the hole-only devices with the architecture of FTO/PEDOT:PSS/perovskite/PTAA/Ag. PTAA is poly(triaryl amine).

is equal to the parallel resistance of the equivalent circuit, r_p. At low applied voltage, r_p equates to the shunt resistance across the perovskite layer, estimated at 93, 318, and 550 Ω cm^2 for the control, TM-DHP, and both TM-DHP and maltol treated PSCs, respectively. The increase in shunt resistance correlates with the increase in output current of the PSCs, and confirms the successively improved quality of the treated perovskite films.

Charge carrier recombination mechanisms are reflected by the Shockley diode ideality factor, as determined by the slope of the plot of V_{OC} versus incident light-intensity (Fig. 3e).[55,56] The ideality factor is 1.62, 1.60 for the control and TM-DHP treated devices, respectively, falling to 1.50 for the device treated with both TM-DHP and maltol, indicating lower non-radiative (trap-mediated) recombination rates in the maltol-treated PSCs.

To estimate the density of trap states in the films, we measured the dark current–voltage (I–V) curves of the hole-only and electron-only devices (Fig. 3f). The voltage where the current begins to sharply increase can be assigned to the trap-filled limit voltage (V_{TFL}). V_{TFL} is related to the trap density, N_{trap}, as $V_{TFL} = N_{trap}(eL^2)/(2\varepsilon_r\varepsilon_0)$, where e is the elementary charge of the electron, ε_0 is the vacuum permittivity, ε_r is the relative dielectric constant of the perovskite (around 32),[57] and L is the thickness of the perovskite film. V_{TFL} for the perovskite films in the hole-only devices is 0.62, 0.54, and 0.14 V, respectively, corresponding to trap densities of 2.9×10^{15}, 2.4×10^{15}, and 6.3×10^{14} cm^{-3}. The electron trap densities for the perovskite films modified with TM-DHP and maltol were estimated to be around 3.6×10^{14} cm^{-3} (Table S2, Fig. S19†). These electrical measurements confirm the lower trap-state densities in the treated perovskite films, which leads to longer carrier lifetimes of the treated perovskite films, as well as improved performance of the PSCs.

3. Conclusions

In this study, we found that maltol, a cheap and common flavor enhancer, can coordinate to Sn(II) in SnI$_2$ to form a stable complex (SnI(maltol)). Based on this strong affinity of maltol for Sn(II), we demonstrated that, when used in combination with a Sn(IV) scavenging method acting on the precursor solution, post-treatment with maltol leads to suppressed Sn(IV) content, decreased defect densities, and remarkably prolonged charge carrier lifetimes in the perovskite films, over 7 µs. A PCE of 21.4% was achieved for the champion solar cell. These high quality Pb–Sn materials achieved by the simple post-treatment should be useful for wide variety of optoelectronic devices.

Author contributions

S. H. and A. W. conceived the idea. S. H. and K. O. performed the synthesis and characterization of Sn complexes. S. H. and M. A. T. conducted the XPS measurements. K. O. conducted the XRD measurements. K. O. carried out the PL measurements with help of T. H., T. Y. and Y. K. R. N. and A. S. conducted the TRMC measurements. S. H., M. A. T., and K. O. fabricated and measured the devices, and conducted SEM characterizations with the help of Y. I. S. H. and K. O. carried out the PYS

measurements. R. M. conducted the impedance measurements. S. H. conducted the SCLC measurements with the help of R. M. M. A. T. and K. O. carried out the NMR measurements. S. H., M. A. T., R. M., and A. W. prepared the manuscript. All authors commented on the manuscript. A. W. supervised the project.

Conflicts of interest

There are no conflicts to declare.

Acknowledgements

Notes and references

1 J. J. Yoo, G. Seo, M. R. Chua, T. G. Park, Y. Lu, F. Rotermund, Y.-K. Kim, C. S. Moon, N. J. Jeon, J.-P. Correa-Baena, V. Bulović, S. S. Shin, M. G. Bawendi and J. Seo, *Nature*, 2021, **590**, 587–593.

2 J. Jeong, M. Kim, J. Seo, H. Lu, P. Ahlawat, A. Mishra, Y. Yang, M. A. Hope, F. T. Eickemeyer, M. Kim, Y. J. Yoon, I. W. Choi, B. P. Darwich, S. J. Choi, Y. Jo, J. H. Lee, B. Walker, S. M. Zakeeruddin, L. Emsley, U. Rothlisberger, A. Hagfeldt, D. S. Kim, M. Grätzel and J. Y. Kim, *Nature*, 2021, **592**, 381–385.

3 M. Hu, M. Chen, P. Guo, H. Zhou, J. Deng, Y. Yao, Y. Jiang, J. Gong, Z. Dai, Y. Zhou, F. Qian, X. Chong, J. Feng, R. D. Schaller, K. Zhu, N. P. Padture and Y. Zhou, *Nat. Commun.*, 2020, **11**, 151.

4 W. Shockley and H. J. Queisser, *J. Appl. Phys.*, 1961, **32**, 510–519.

5 M. T. Klug, R. L. Milot, J. B. Patel, T. Green, H. C. Sansom, M. D. Farrar, A. J. Ramadan, S. Martani, Z. Wang, B. Wenger, J. M. Ball, L. Langshaw, A. Petrozza, M. B. Johnston, L. M. Herz and H. J. Snaith, *Energy Environ. Sci.*, 2020, **13**, 1776–1787.

6 A. Goyal, S. McKechnie, D. Pashov, W. Tumas, M. van Schilfgaarde and V. Stevanović, *Chem. Mater.*, 2018, **30**, 3920–3928.

7 J. Tong, Z. Song, D. H. Kim, X. Chen, C. Chen, A. F. Palmstrom, P. F. Ndione, M. O. Reese, S. P. Dunfield,
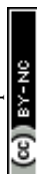
O. G. Reid, J. Liu, F. Zhang, S. P. Harvey, Z. Li, S. T. Christensen, G. Teeter, D. Zhao, M. M. Al-Jassim, M. F. A. M. van Hest, M. C. Beard, S. E. Shaheen, J. J. Berry, Y. Yan and K. Zhu, *Science*, 2019, **364**, 475.

8 T. Jiang, Z. Chen, X. Chen, T. Liu, X. Chen, W. E. I. Sha, H. Zhu and Y. Yang, *Sol. RRL*, 2020, **4**, 1900467.

9 R. Lin, K. Xiao, Z. Qin, Q. Han, C. Zhang, M. Wei, M. I. Saidaminov, Y. Gao, J. Xu, M. Xiao, A. Li, J. Zhu, E. H. Sargent and H. Tan, *Nat. Energy*, 2019, **4**, 864–873.

10 C. Li, Z. Song, D. Zhao, C. Xiao, B. Subedi, N. Shrestha, M. M. Junda, C. Wang, C.-S. Jiang, M. Al-Jassim, R. J. Ellingson, N. J. Podraza, K. Zhu and Y. Yan, *Adv. Energy Mater.*, 2019, **9**, 1803135.

11 J. Xi and M. A. Loi, *ACS Energy Lett.*, 2021, **6**, 1803–1810.

12 K. Xiao, R. Lin, Q. Han, Y. Hou, Z. Qin, H. T. Nguyen, J. Wen, M. Wei, V. Yeddu, M. I. Saidaminov, Y. Gao, X. Luo, Y. Wang, H. Gao, C. Zhang, J. Xu, J. Zhu, E. H. Sargent and H. Tan, *Nat. Energy*, 2020, **5**, 870–880.

13 G. Kapil, T. Bessho, T. Maekawa, A. K. Baranwal, Y. Zhang, M. A. Kamarudin, D. Hirotani, Q. Shen, H. Segawa and S. Hayase, *Adv. Energy Mater.*, 2021, **11**, 2101069.

14 G. Kapil, T. Bessho, C. H. Ng, K. Hamada, M. Pandey, M. A. Kamarudin, D. Hirotani, T. Kinoshita, T. Minemoto, Q. Shen, T. Toyoda, T. N. Murakami, H. Segawa and S. Hayase, *ACS Energy Lett.*, 2019, **4**, 1991–1998.

15 Z. Yang, Z. Yu, H. Wei, X. Xiao, Z. Ni, B. Chen, Y. Deng, S. N. Habisreutinger, X. Chen, K. Wang, J. Zhao, P. N. Rudd, J. J. Berry, M. C. Beard and J. Huang, *Nat. Commun.*, 2019, **10**, 4498.

16 M. Wei, K. Xiao, G. Walters, R. Lin, Y. Zhao, M. I. Saidaminov, P. Todorović, A. Johnston, Z. Huang, H. Chen, A. Li, J. Zhu, Z. Yang, Y.-K. Wang, A. H. Proppe, S. O. Kelley, Y. Hou, O. Voznyy, H. Tan and E. H. Sargent, *Adv. Mater.*, 2020, **32**, 1907058.

17 W. Ke, C. Chen, I. Spanopoulos, L. Mao, I. Hadar, X. Li, J. M. Hoffman, Z. Song, Y. Yan and M. G. Kanatzidis, *J. Am. Chem. Soc.*, 2020, **142**, 15049–15057.

18 C. Li, Z. Song, C. Chen, C. Xiao, B. Subedi, S. P. Harvey, N. Shrestha, K. K. Subedi, L. Chen, D. Liu, Y. Li, Y.-W. Kim, C.-s. Jiang, M. J. Heben, D. Zhao, R. J. Ellingson, N. J. Podraza, M. Al-Jassim and Y. Yan, *Nat. Energy*, 2020, **5**, 768–776.

19 R. Prasanna, T. Leijtens, S. P. Dunfield, J. A. Raiford, E. J. Wolf, S. A. Swifter, J. Werner, G. E. Eperon, C. de Paula, A. F. Palmstrom, C. C. Boyd, M. F. A. M. van Hest, S. F. Bent, G. Teeter, J. J. Berry and M. D. McGehee, *Nat. Energy*, 2019, **4**, 939–947.

20 J. Tong, J. Gong, M. Hu, S. K. Yadavalli, Z. Dai, F. Zhang, C. Xiao, J. Hao, M. Yang, M. A. Anderson, E. L. Ratcliff, J. J. Berry, N. P. Padture, Y. Zhou and K. Zhu, *Matter*, 2021, **4**, 1365–1376.

21 E. Ruggeri, M. Anaya, K. Gałkowski, G. Delport, F. U. Kosasih, A. Abfalterer, S. Mackowski, C. Ducati and S. D. Stranks, *Adv. Mater.*, 2019, **31**, 1905247.

22 F. Li, X. Deng, F. Qi, Z. Li, D. Liu, D. Shen, M. Qin, S. Wu, F. Lin, S.-H. Jang, J. Zhang, X. Lu, D. Lei, C.-S. Lee, Z. Zhu and A. K. Y. Jen, *J. Am. Chem. Soc.*, 2020, **142**, 20134–20142.

23 A. Y. Alsalloum, B. Turedi, K. Almasabi, X. Zheng, R. Naphade, S. D. Stranks, O. F. Mohammed and O. M. Bakr, *Energy Environ. Sci.*, 2021, **14**, 2263–2268.

24 S. Wu, Z. Li, M.-Q. Li, Y. Diao, F. Lin, T. Liu, J. Zhang, P. Tieu, W. Gao, F. Qi, X. Pan, Z. Xu, Z. Zhu and A. K. Y. Jen, *Nat. Nanotechnol.*, 2020, **15**, 934–940.

25 M. I. Saidaminov, I. Spanopoulos, J. Abed, W. Ke, J. Wicks, M. G. Kanatzidis and E. H. Sargent, *ACS Energy Lett.*, 2020, **5**, 1153–1155.

26 J. Pascual, G. Nasti, M. H. Aldamasy, J. A. Smith, M. Flatken, N. Phung, D. Di Girolamo, S.-H. Turren-Cruz, M. Li, A. Dallmann, R. Avolio and A. Abate, *Mater. Adv.*, 2020, **1**, 1066–1070.

27 T.-B. Song, T. Yokoyama, C. C. Stoumpos, J. Logsdon, D. H. Cao, M. R. Wasielewski, S. Aramaki and M. G. Kanatzidis, *J. Am. Chem. Soc.*, 2017, **139**, 836–842.

28 T.-B. Song, T. Yokoyama, S. Aramaki and M. G. Kanatzidis, *ACS Energy Lett.*, 2017, **2**, 897–903.

29 F. Wang, J. Ma, F. Xie, L. Li, J. Chen, J. Fan and N. Zhao, *Adv. Funct. Mater.*, 2016, **26**, 3417–3423.

30 Q. Chen, J. Luo, R. He, H. Lai, S. Ren, Y. Jiang, Z. Wan, W. Wang, X. Hao, Y. Wang, J. Zhang, I. Constantinou, C. Wang, L. Wu, F. Fu and D. Zhao, *Adv. Energy Mater.*, 2021, **11**, 2101045.

31 K. J. Savill, A. M. Ulatowski and L. M. Herz, *ACS Energy Lett.*, 2021, **6**, 2413–2426.

32 L. Xu, X. Feng, W. Jia, W. Lv, A. Mei, Y. Zhou, Q. Zhang, R. Chen and W. Huang, *Energy Environ. Sci.*, 2021, **14**, 4292–4317.

33 F. Gu, S. Ye, Z. Zhao, H. Rao, Z. Liu, Z. Bian and C. Huang, *Sol. RRL*, 2018, **2**, 1800136.

34 S. J. Lee, S. S. Shin, Y. C. Kim, D. Kim, T. K. Ahn, J. H. Noh, J. Seo and S. I. Seok, *J. Am. Chem. Soc.*, 2016, **138**, 3974–3977.

35 Q. Tai, X. Guo, G. Tang, P. You, T.-W. Ng, D. Shen, J. Cao, C.-K. Liu, N. Wang, Y. Zhu, C.-S. Lee and F. Yan, *Angew. Chem., Int. Ed.*, 2019, **58**, 806–810.

36 Z. Lin, C. Liu, G. Liu, J. Yang, X. Duan, L. Tan and Y. Chen, *Chem. Commun.*, 2020, **56**, 4007–4010.

37 M. Ozaki, Y. Katsuki, J. Liu, T. Handa, R. Nishikubo, S. Yakumaru, Y. Hashikawa, Y. Murata, T. Saito, Y. Shimakawa, Y. Kanemitsu, A. Saeki and A. Wakamiya, *ACS Omega*, 2017, **2**, 7016–7021.

38 J. Liu, M. Ozaki, S. Yakumaru, T. Handa, R. Nishikubo, Y. Kanemitsu, A. Saeki, Y. Murata, R. Murdey and A. Wakamiya, *Angew. Chem., Int. Ed.*, 2018, **57**, 13221–13225.

39 T. Nakamura, T. Handa, R. Murdey, Y. Kanemitsu and A. Wakamiya, *ACS Appl. Electron. Mater.*, 2020, **2**, 3794–3804.

40 T. Nakamura, S. Yakumaru, M. A. Truong, K. Kim, J. Liu, S. Hu, K. Otsuka, R. Hashimoto, R. Murdey, T. Sasamori, H. D. Kim, H. Ohkita, T. Handa, Y. Kanemitsu and A. Wakamiya, *Nat. Commun.*, 2020, **11**, 3008.

41 D. Luo, X. Li, A. Dumont, H. Yu and Z. H. Lu, *Adv. Mater.*, 2021, **33**, e2006004.

42 J. Xue, R. Wang and Y. Yang, *Nat. Rev. Mater.*, 2020, **5**, 809–827.

43 M. A. Kamarudin, D. Hirotani, Z. Wang, K. Hamada, K. Nishimura, Q. Shen, T. Toyoda, S. Iikubo, T. Minemoto,

K. Yoshino and S. Hayase, *J. Phys. Chem. Lett.*, 2019, **10**, 5277–5283.

44 W. Ke, C. C. Stoumpos and M. G. Kanatzidis, *Adv. Mater.*, 2019, **31**, 1803230.

45 S. Shahbazi, M.-Y. Li, A. Fathi and E. W.-G. Diau, *ACS Energy Lett.*, 2020, **5**, 2508–2511.

46 M. C. Barret, M. F. Mahon, K. C. Molloy, J. W. Steed and P. Wright, *Inorg. Chem.*, 2001, **40**, 4384–4388.

47 J. Xue, R. Wang, K.-L. Wang, Z.-K. Wang, I. Yavuz, Y. Wang, Y. Yang, X. Gao, T. Huang, S. Nuryyeva, J.-W. Lee, Y. Duan, L.-S. Liao, R. Kaner and Y. Yang, *J. Am. Chem. Soc.*, 2019, **141**, 13948–13953.

48 T. Wu, Y. Wang, X. Li, Y. Wu, X. Meng, D. Cui, X. Yang and L. Han, *Adv. Energy Mater.*, 2019, **9**, 1803766.

49 H. Zhang, Y. Wu, C. Shen, E. Li, C. Yan, W. Zhang, H. Tian, L. Han and W.-H. Zhu, *Adv. Energy Mater.*, 2019, **9**, 1803573.

50 Y. Yamada, T. Nakamura, M. Endo, A. Wakamiya and Y. Kanemitsu, *J. Am. Chem. Soc.*, 2014, **136**, 11610–11613.

51 Y. Liu, Y. Zhang, X. Zhu, Z. Yang, W. Ke, J. Feng, X. Ren, K. Zhao, M. Liu, M. G. Kanatzidis and S. Liu, *Sci. Adv.*, 2021, **7**, eabc8844.

52 L. Gao, K. Zeng, J. Guo, C. Ge, J. Du, Y. Zhao, C. Chen, H. Deng, Y. He, H. Song, G. Niu and J. Tang, *Nano Lett.*, 2016, **16**, 7446–7454.

53 N. Ishida, A. Wakamiya and A. Saeki, *ACS Photonics*, 2016, **3**, 1678–1688.

54 E. M. Hutter, J.-J. Hofman, M. L. Petrus, M. Moes, R. D. Abellón, P. Docampo and T. J. Savenije, *Adv. Energy Mater.*, 2017, **7**, 1602349.

55 P. Caprioglio, C. M. Wolff, O. J. Sandberg, A. Armin, B. Rech, S. Albrecht, D. Neher and M. Stolterfoht, *Adv. Energy Mater.*, 2020, **10**, 2000502.

56 T. S. Sherkar, C. Momblona, L. Gil-Escrig, J. Ávila, M. Sessolo, H. J. Bolink and L. J. A. Koster, *ACS Energy Lett.*, 2017, **2**, 1214–1222.

57 Q. Dong, Y. Fang, Y. Shao, P. Mulligan, J. Qiu, L. Cao and J. Huang, *Science*, 2015, **347**, 967.